



Review

# Electronic process of Cu(Ag, V, Rh)(0 0 1) surface oxidation: atomic valence evolution and bonding kinetics

Chang Q. Sun\*

*School of Electrical and Electronic Engineering, Nanyang Technological University,  
Nanyang Avenue, Singapore 639798, Singapore*

Received 26 June 2004; accepted 12 November 2004

Available online 19 December 2004

## Abstract

The electronic processes of Cu(Ag, V, Rh)(0 0 1) surface oxidation are comparatively analyzed based on the recent ‘chemical bond–valence band–potential barrier’ (BBB) correlation mechanism [C.Q. Sun, *Prog. Mater. Sci.* 48, 521–685 (2003)], which allows reaction formulae for all the observed phases with identification of individual atomic valence and the binding kinetics at the surfaces with the same geometry. It is consistently understood that the forming kinetics of the primary oxide tetrahedron and its derivative on the valence density-of-states (DOS) are intrinsically common for all these analyzed systems, though the patterns of observation in terms of morphology and crystallography vary from situation to situation. However, the lattice size and electronegativity of the host surfaces determine extrinsically the site selectivity of the oxygen, the order of bond formation and the orientation of the oxide tetrahedron.

© 2004 Elsevier B.V. All rights reserved.

*Keywords:* Chemical bond; Valence band; Surface potential; Cu; Ag; V; Rh; Oxygen; Oxidation; Reaction kinetics; Scanning tunneling microscopy; LEED; PES

## 1. Introduction

Oxygen chemisorption onto the fcc(0 0 1) surface of transition metals of Cu and V, and noble metals of Ag and Rh have attracted tremendous interest over the past decades because the mechanism behind the observations is of utmost importance for improvements in traditional industry branches such as

corrosion protection and catalytic applications as well as for innovation in upcoming technological fields such as nanostructuring of surfaces for device fabrication. As a consequence, many experimental and theoretical groups all over the world are involved in this field to clarify the key issues such as charge transportation, atomic valence alteration and bonding kinetics upon reaction. Unfortunately, progress made has hitherto not very satisfactory as these issues are often beyond the scope of direct observations using the state-of-the-art technologies. Here, we show that from

\* Tel.: +65 6790 4517; fax: +65 6792 0415.

E-mail address: [ecqsun@ntu.edu.sg](mailto:ecqsun@ntu.edu.sg).

the perspective of bond formation and its consequence on the valence electrons and surface potential (bond–band–barrier (BBB) correlation) [1], we could advance a consistent and deeper understanding of the key issues of these systems.

Generally, oxygen interacting with the fcc(0 0 1) surface of Cu, Ag, V, and Rh produces versatile patterns as observed using scanning tunneling microscopy (STM) and low-energy-electron diffraction (LEED). It is common that oxygen adsorption induces two sequential phases on these fcc(0 0 1) surfaces and that the first layer spacing expands and the second contracts upon oxygen being up-taken despite the vertical adsorbate positions of which the accuracy is always the focus of debate. The O–Cu(0 0 1) [2] and O–Rh(0 0 1) [3] surface oxidation have been well and consistently understood in terms of the BBB correlation. The evolution of  $O^{1-}$  to  $O^{2-}$  with oxide quasi-tetrahedron formation creates the  $(2 \times 2)\text{-}2O^{1-}$  phase consisting of  $\text{CuO}_2$  pairing pyramid (Fig. 1a) and then the  $(\sqrt{2} \times 2\sqrt{2})R45^\circ\text{-}2O^{2-}$  phase composed of  $\text{Cu}_3\text{O}_2$  pairing tetrahedron at the Cu(0 0 1) surface (Fig. 1b). The evolution of  $O^{1-}$  to  $O^{2-}$  also switches the  $(2 \times 2)\text{-}2O^{1-}$  ‘radial’ reconstruction (Fig. 1c) with  $O^{1-}$  preferring the five-fold-coordinated site into the  $(2 \times 2)p4g\text{-}2O^{2-}$  ‘clock’ reconstruction pattern with ‘rhombi-chain’ running along the  $\langle 1 1 \rangle$  direction at the Rh(0 0 1) surface (Fig. 1d). However, mechanism remains yet poorly known for the oxygen to induce the sequential phases on the Ag(0 0 1) and the V(0 0 1) surfaces. Theoretical and experimental observations revealed that the first O–Ag(0 0 1) phase is the same as the fcc(0 0 1)– $(2 \times 2)\text{-}2O^{1-}$  of Rh showing ‘radial’ pattern of reconstruction; the second O–Ag(0 0 1) low-temperature phase is the same as the missing-row type Cu(0 0 1)– $(\sqrt{2} \times 2\sqrt{2})R45^\circ\text{-}2O^{2-}$  reconstruction. Unlike the O–Cu(0 0 1) surface of which the phase transition occurs at a temperature that is higher than ambient temperature ( $\sim 700$  K), the O–Ag(0 0 1) phase transition takes place at temperature ( $\sim 240$  K) that is much lower in an inverse phase order (from  $O^{1-}$  to  $O^{2-}$  when the temperature drops). It is also a puzzle that oxygen induces the same fcc(0 0 1)– $(2 \times 2)\text{-}2O^{1-}$  phase and then a short-ordered  $(1 \times 5)$  structures at the V(0 0 1) surface (STM image shown in Fig. 1e). Therefore, it is essential to find what is common, what is uncommon and how the common stuff performs uncommonly at these surfaces with the

same fcc(0 0 1) geometry, and hence to unify the versatile patterns of observations of these systems. Here, we show that these observations can be unified in terms of bond making and its consequences on the atomic valences and the valence density-of-states (DOS). Besides, we suggest that the accuracy of the static atomic positions determined using diffraction might not be necessary as the reaction is a kinetic process in which the atomic sizes and the atomic valences change continuously. The positions of the involved host and guest atoms dislocate collectively. More importantly, charge polarization and charge transportation dominate the electronic process of reaction and hence, our focus should be more on the electronic process of oxidation than on the crystal geometry of the adsorbed systems.

## 2. Principle: BBB correlation

The BBB correlation mechanism was developed based on calculations of very low-energy-electron-diffraction (VLEED) from Cu(0 0 1) surface with oxygen adsorption under various conditions [2]. The BBB correlation has also been intensively verified with other approaches such as photoelectron emission (PES), thermal desorption (TDS), electron energy loss (EELS), Raman spectroscopy, and STM/S from other systems with chemisorbed oxygen. The BBB correlation indicates that it is necessary for an oxygen atom to hybridize its sp-orbitals upon interacting with a solid surface. In the process of oxidation, the oxide bond forming in four discrete stages (see inset in Fig. 1d) [1]: one bond forms first and then the other follows; the sp-orbital of an O atom then hybridizes with creation of nonbonding lone pairs that induce antibonding dipoles. Overdosing O to the system, H-like bond forms that turns the ‘dipole’ into ‘dipole/+’ and the polarized electrons will flow into the bonding orbital of the O atom (arrow from antibonding to bonding state in Fig. 1f). These atomic valences add corresponding density-of-states features to the valence band and above of the host, which dictate the performance of a system with oxygen being involved. On the other hand, charge transport from the metal atom to oxygen for bonding, or polarization, leaves holes behind which generates a gap, or widens the existing gap, between the conduction band and

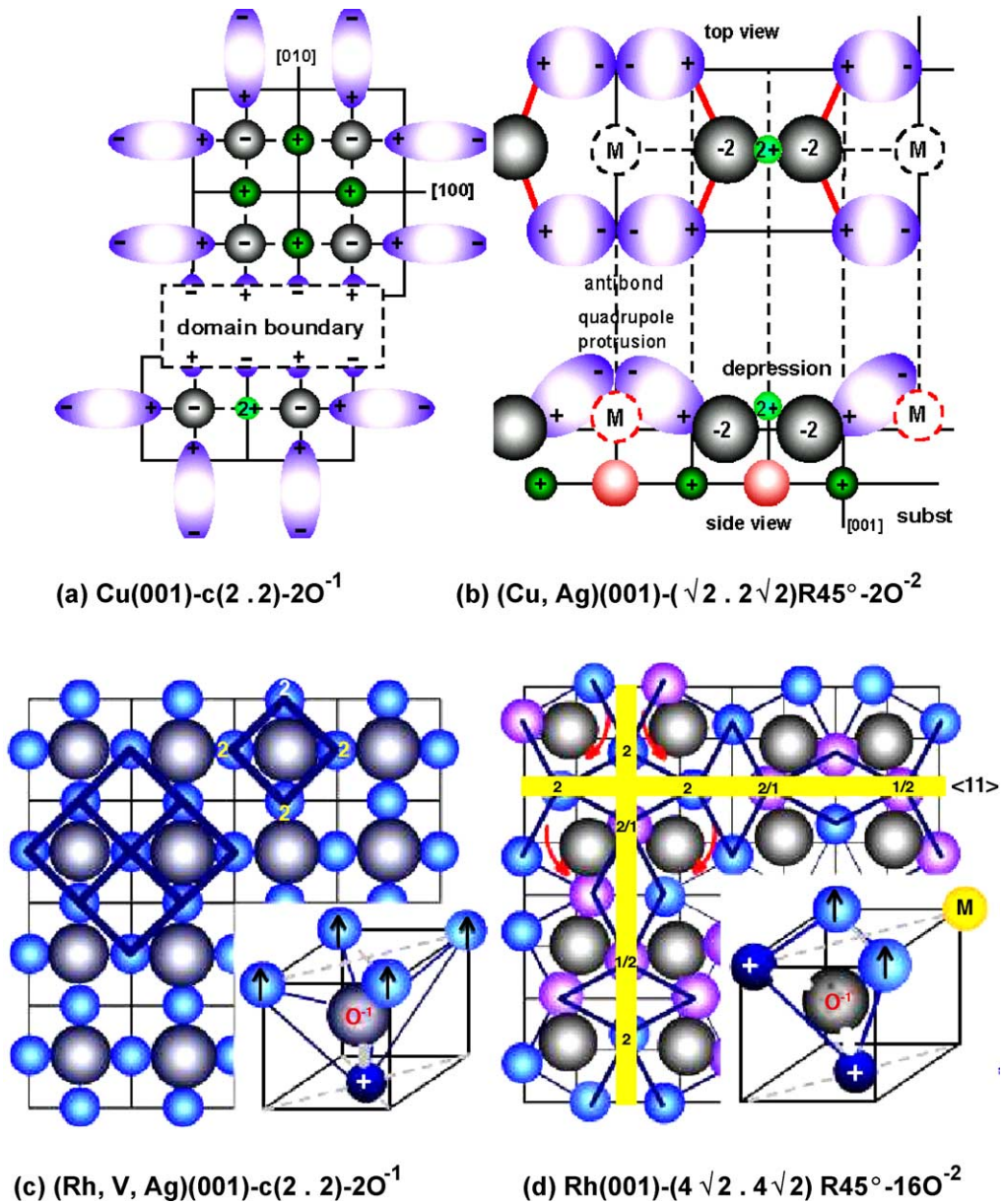


Fig. 1. Models for O-(Cu, Rh, Ag, V)(0 0 1) surface chemistry and oxygen-derived DOS features. (a) Short ordered Cu(0 0 1)- $c(2 \times 2)\text{-}2\text{O}^{-1}$  phase is composed of CuO (upper domain) or  $\text{Cu}_2\text{O}$  (lower domain) off-centered pyramid of which the  $\text{O}^{1-}$  sits  $\sim 0.04$  nm above the Cu top plane and shifts  $\sim 0.018$  nm off the  $\text{C}_{4v}$  hollow center. (b)  $(\text{Cu, Ag})(0 0 1)\text{-}(\sqrt{2} \times \sqrt{2})\text{R}45^\circ\text{-}2\text{O}^{-2}$  phase consists  $\text{Cu}_3\text{O}_2$  pairing tetrahedron. The pairing dipoles cross over the missing Cu rows (labeled M). (c)  $(\text{Rh, V, Ag})(0 0 1)\text{-}c(2 \times 2)\text{-}2\text{O}^{-1}$  structure contains  $\text{O}^{1-}$  sitting inside the next nearest  $\text{C}_{4v}$  hollow (inset shows the primary structure). (d)  $\text{Rh}(0 0 1)\text{-}(4\sqrt{2} \times 4\sqrt{2})\text{R}45^\circ\text{-}16\text{O}^{-2}$  phase corresponds to the ‘clock’ reconstruction and the rhombi-chain along the  $\langle 11 \rangle$  direction. The inset quasi-tetrahedron forms commonly the primary unit for all the  $\text{O}^{2-}$  derived phases. (e) Short ordered V(0 0 1)- $(\sqrt{2} \times \sqrt{2})\text{R}45^\circ\text{-}4\text{O}^{-2}$  phase involves H-like bond (dipole  $\rightarrow \text{O}^{2-}$ ) that stabilizes the system by lowering the STM protrusions and restores the work function reduction. (f) O-derived DOS features of bonding ( $\ll E_F$ ), nonbonding (lone pair) ( $< E_F$ ), antibonding (dipole) ( $> E_F$ ) and holes ( $\leq E_F$ ). Antibond dipoles contribute to STM high protrusions and the reduction of work function ( $\phi_0 \rightarrow \phi_1$ ). Hole production creates band gap and turns metals to be semiconductors.

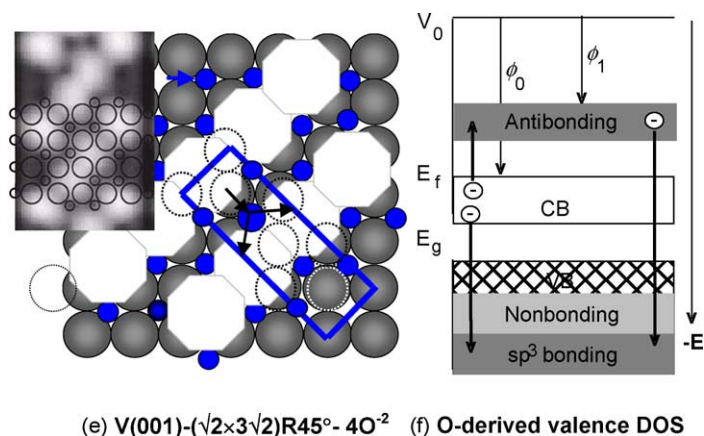
(e)  $V(001)-(\sqrt{2}\times\sqrt{3}/\sqrt{2})R45^\circ-4O^{2-}$  (f) O-derived valence DOS

Fig. 1. (Continued).

the valence band. Antibonding dipole formation due to polarization lowers the surface work function, which is also true for oxygen penetrating into the bulk to polarize the metal by the  $O^{1-}$  or the lone electron pairs. Bond forming also alters the sizes and valencies of the involved atoms and causes a collective dislocation of these atoms, which corrugate the morphology or the surface potential barrier (SPB) as identified with STM imaging and VLEED calculations. Therefore, it is possible for us to derive the individual atomic valence at the surface from STM/S, UPS, and LEED observations or observations by other means such as thermal desorption, and hence to obtain comprehensive information about the bond forming kinetics and its consequence on the behavior of valence electrons and the surface atoms.

Based on the BBB correlation, identities probed with techniques such as STM/S, LEED, PES, and TDS have been consistently defined in terms of atomic valences, bond geometry, valence DOS, bond strength, and bond forming kinetics [1]. The process of the low-index surfaces of transition metals Cu and Co, noble metals Rh, Ru, Pd, and non-metallic diamond [4] have been consistently formulated in terms of atomic valences and bonding kinetics. The BBB correlation has also been extended to the reactions of Ni(0 0 1) with carbon and nitrogen, which has led to a novel approach neutralizing the diamond–metal interfacial stress and hence strengthening the diamond–metal adhesion substantially [5]. The mechanism of band-gap generation has also enabled design and fabrication

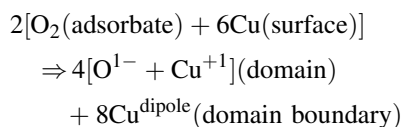
of PbZrTi oxide that emits intense and stable blue light [6]. Progress insofar evidences sufficiently the reality and validity of the BBB correlation mechanism that is helpful in understanding C, N, and O reaction and it is useful in technical applications such as material design. The BBB correlation and its practical applications have formed the subject of a recent featured report [1]. This communication focuses on the electronic process of fcc(0 0 1) surface oxidation towards the mechanism that is common behind various observations of these surfaces of the same geometry.

### 3. Analysis

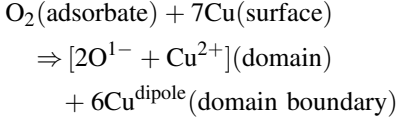
#### 3.1. $O-Cu(0\ 0\ 1)$ and $O-Rh(0\ 0\ 1)$

Knowledge about the atomic valencies, phase structures, bond geometry, bond forming kinetics, and the driving force for  $O-Cu(0\ 0\ 1)$  [7] and  $O-Rh(0\ 0\ 1)$  [8] surface reaction has been summarized in refs. [2,3]. Briefly, the complete process of  $O-Cu(0\ 0\ 1)$  reaction follows the relation:

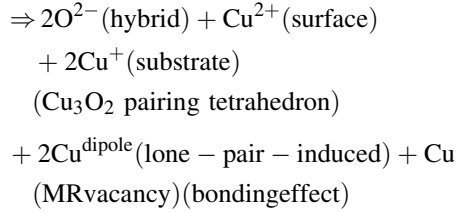
The upper  $(2\sqrt{2} \times 2\sqrt{2})R45^\circ-4O^{1-}$  domain in Fig. 1a is composed of  $Cu_4O$  off-centered pyramid:



or for the lower  $(\sqrt{2} \times 2\sqrt{2})R45^\circ-2O^{1-}$  domain that comprises  $CuO_2$  pairing pyramid:



Upon increasing oxygen,  $O^{1-}$  evolves into  $O^{2-}$ , giving rise to the well-known missing-row (MR) type reconstruction (Fig. 1b):



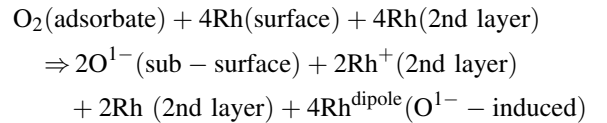
In the first phase, the  $[2O^{1-} + Cu^{2+}]$  or the  $4[O^{1-} + Cu^{+1}]$  clusters form the depressed domains; the  $O^{1-}$ -induced  $Cu^{\text{dipole}}$  that buckles up to form the ‘engaged-cogwheels’ domain boundaries that are detected as patches of protrusion in STM imaging [9]. The surface is fully covered with dipoles (alternative signs of charge distribution) in a way that it stabilizes not only the domains but also the domain boundaries. In this phase, the surface stress should be tensile though further confirmation may be necessary. According to VLEED optimization [2], the  $O^{1-}$  adsorbate locates  $\sim 0.04$  nm above the surface with a  $\sim 0.018$  nm off-centered shift towards the  $Cu^{2+}$ .

Upon increasing oxygen-exposure, the ‘disordered’ nanometric  $c(2 \times 2)-2O^{1-}$  domain develops into the ‘ordered’  $(\sqrt{2} \times 2\sqrt{2})R45^\circ-2O^{2-}$  phase in which every fourth row of Cu atoms is missing [10,11]. The  $Cu(001)$  surface geometry allows the  $Cu_3O_2$  pairing tetrahedron to form in such a way that one Cu atom in the substrate is involved (Fig. 1b). The top layer of the  $(\sqrt{2} \times \sqrt{2})R45^\circ-2O^{2-}$  phase contains rows of  $Cu^{2+}$ , a pairing  $[O^{2-}:Cu^{\text{dipole}}:O^{2-}]$  row zigzagged ( $140^\circ$  or more) by the lone pairs ‘:’ and the MR vacancy. In the second phase, the surface stress should be compressive due to the repulsion among the surface dipoles.

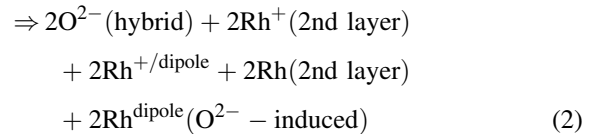
VLEED calculations revealed that the work function is reduced by 1.2 eV and the muffin-tin inner potential constant is decreased by  $\sim 10\%$  (from 11.56 to 10.5 eV) upon the  $Cu(001)$  surface being oxidized. A DOS feature appeared around 1–.5 eV

below  $E_F$  in the second phase corresponding to the nonbonding lone pair states. The shape of the SPB varies from site to site on the surface. The  $Cu^{\text{dipole}}$  that enhances the SPB through the outward shift and saturation of the wave function corresponds to the STM protrusion, while the ions ( $Cu^+$  and  $O^{1-}$  and  $O^{2-}$ ) correspond to depressions. In the process of oxidation,  $O-Cu(001)$  surface bond forms in four discrete stages [12]: first, upon dissociation, O atom deposits on the surface with one contraction (by 12% to 0.163 nm) ionic bond forming between the O and a Cu atom on the surface (Fig. 1a). Second, another contracting  $O-Cu$  bond (by 4% to 0.176 nm) follows between the oxygen and a Cu in the substrate (Fig. 1b). As a result, the oxygen adsorbate buckles into the bulk. Then, the ionic bond angle increases to a saturation value of  $102^\circ$  or less, leading to the relaxation of layer spacing by 8% (from 1.80 to 0.194 nm). Finally, interaction develops between the lone pairs of oxygen and the lone-pair-induced  $Cu^{\text{dipole}}$  (shifts towards the MR by 0.025 (at  $\Theta \sim 200$  L)  $\sim 0.045$  nm (at  $\Theta \geq 800$  L)). The MR forms prior to transiting the  $O^{1-} \rightarrow O^{2-}$  due to the isolation and polarization. The  $O^{2-}:Cu^{\text{dipole}}$  distance is  $\sim 0.194$  nm. The  $O^{2-}-Cu^{2+}$  bond length is 0.163 nm. The angle between the two bonds is  $104^\circ$  and the angle between the two lone pairs is  $140^\circ$ .

The  $c(2 \times 2)-2O^{1-}$  ‘radial’ and the subsequent  $(2 \times 2)p4g-2O^{2-}$  ‘clock’ reconstruction [13,14] of the  $Rh(001)$  surface can be formulated as follows (Fig. 1c and d):



and then:



In the  $c(2 \times 2)-2O^{1-}$  precursor phase, oxygen sinks into the  $C_{4v}$  hollow site and bonds to the Rh atom underneath forming a  $Rh_5O$  cluster. The  $O^{1-}$  polarizes and pushes the electron cloud of the surface atoms radially away from the central adsorbate. In the second phase, the  $Rh_5O$  pyramid evolves into an

Rh<sub>4</sub>O tetrahedron with an off-centered shift of the adsorbate in the hollow. The tetrahedron defines one Rh<sup>+</sup> (labeled 1) and two lone-pair-induced Rh<sup>dipole</sup> dipoles (labeled 2) of the four nearest surface neighbors (inset in Fig. 1d). The Rh<sub>5</sub>O → Rh<sub>4</sub>O transition gives rise to the overall ‘p4g’, or a  $c(4\sqrt{2} \times 4\sqrt{2})R45^\circ-16O^{2-}$  reconstruction with half Rh<sup>dipole</sup> and another half Rh<sup>+dipole</sup> and rhombi-chain along the  $\langle 1\ 1 \rangle$  direction. The alternative repulsion–attraction along the  $\langle 1\ 1 \rangle$  direction offers the forces that drive the clock rotation and the atomic dislocation is stabilized by the response of tensile bond stress estimated at 35 dyn per bond [3].

### 3.2. O–Ag(0 0 1) and O–V(0 0 1)

At low-temperature, the O–Ag(0 0 1) surface displays a  $c(2 \times 2)$  LEED pattern with an EELS peak at 37 meV [15]. It is intriguing to note that raising the temperature from 180 to 300 K transits the  $c(2 \times 2)$  to a  $(1 \times 1)$  LEED pattern, and shifts the EELS peak from 37 to 30 meV. Rocca et al. [16] has confirmed the phase transition with refined atomic structures. At high-temperature, atomic oxygen sits in the four-fold hollow site, being the same as the Rh(0 0 1)– $c(2 \times 2)$ – $2O^{1-}$  phase (Fig. 1c), while at low-temperature the substrate undergoes a  $(\sqrt{2} \times 2\sqrt{2})R45^\circ$  missing-row type reconstruction that is the same as the Cu(0 0 1)– $(\sqrt{2} \times 2\sqrt{2})R45^\circ-2O^{2-}$  phase (Fig. 1b). In the second phase, oxygen atoms sit in the hollow sites near the Ag missing rows of the substrate, thus giving rise to a  $c(2 \times 2)$  LEED pattern. A density functional theory (DFT) calculation [17] suggested that the missing-row reconstruction is almost degenerate in energy with the non-reconstructed  $c(2 \times 2)$  structure, both of which share the same LEED pattern. Therefore, it is hard to discriminate these two degenerated phases in DFT calculations. However, the O deposition into the surface C<sub>4v</sub> hollow site and the sub-surface five-fold-coordinated hollow site are most stable, practically degenerated, and separated by an energy barrier of ~25 meV or less. Similarly, the first Ag interlayer spacing expands by up to 30% upon oxygen adsorption [18].

Investigation using STM, LEED, and DFT approaches [18] reveals that the O–V(0 0 1) surface reconstruction undergoes biphasic structure formation in addition to the visible dark lines, separated by 4–6

$\langle 1\ 0 \rangle$ -lattice constants, arranged regularly at the surface along the  $\langle 1\ 0 \rangle$  directions. Simulated STM images revealed that the first phase within the  $(1 \times 5)$  domain is exactly the same as the Rh(0 0 1)– $c(2 \times 2)$ – $2O^{1-}$  phase (Fig. 1c). Auger electron spectroscopy (AES) detected oxygen coverage as 2/3 ML. With increasing the coverage to ~0.73 ML, the second phase appears (see STM image as inset in Fig. 1e) in which the regular dark lines remain. The short-ordered and zigzagged ‘O–O’ chains run along the  $\langle 1\ 1 \rangle$  direction. DFT calculations at very low oxygen coverage revealed that the four-fold hollow sited oxygen along the dark lines is energetically most favorable (–4.89 eV) compared to other sites. LEED optimization [18] with a total number of 26 independent parameters leads to a structural model for the second phase (with R-factor value of 0.17), which is inconsistent with the models derived from STM imaging and DFT optimization. Both the LEED and DFT optimization revealed an expansion of the first layer spacing (+4.2%) and a contraction of the second (–3.2%) with respect to the clean V(0 0 1) surface that contracts by ~–8.5% (LEED) or –15% (DFT). The optimal structures (–5.26 eV) at higher oxygen coverage, as shown in Fig. 1e, may be suggested as a short-ordered V(0 0 1)– $(\sqrt{2} \times 3\sqrt{2})R45^\circ-4O^{2-}$  (2/3 ML).

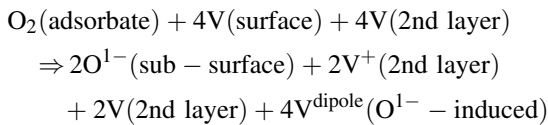
The striking difference between the O–Cu(0 0 1) and the O–Ag(0 0 1) surface are the temperature of phase transition and the inverse phase order. The O–Cu(0 0 1) missing row structure forms and stabilizes at ~700 K at higher oxygen exposure while the O–Ag(0 0 1) missing row structure forms and stabilizes at 300 K or lower at lower exposure. XPS profiles [16] show that the O 1s lower binding energy (–528.3 eV) component increases its intensity with temperature rise at an expense of decreasing the high binding energy (–530.9 eV) that dominates at  $T \leq 300$  K. This is also in line with the 37 → 30 meV transition of EELS vibration. The transition of the XPS binding energy and the EELS stretching vibration evidences that the O–Ag(0 0 1) surface undergoes a transition from stable to quasi-stable as temperature rises. At 246 K, the stable phase forms gradually with about 3200 s aging time. With oxygen adsorption, an additional DOS feature at –2.0 to –3.0 eV emerges [16,19], which agrees with that observed from the O–Ag(1 1 0) (–1.5 to –3.3 eV) [20], O–Ag(1 1 1)

(−2.0 eV) [21], O–Cu(0 0 1) [22,23], O–Rh(0 0 1) [24], and other oxide surfaces [25]. It has been clear that such features arise from lone electron pairs of the sp-hybridized oxygen.

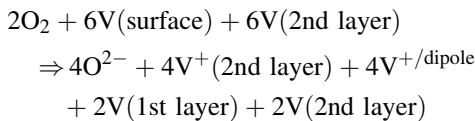
Formulae of reaction kinetics and the surface atomic valencies alteration of the O–Ag(0 0 1) phases follow that of the O–Rh(0 0 1) first phase and that of the O–Cu(0 0 1) second phase, respectively. The transition of XPS O 1s peak and the EELS feature are indication of oxygen de-hybridization at around 246 K. O<sup>2−</sup> and its derivatives at lower temperature appear to be more stable than the O<sup>1−</sup>, according to the XPS and EELS spectral features [15,18]. Therefore, this intriguing low-temperature Ag<sub>5</sub>O → Ag<sub>3</sub>O<sub>2</sub> transition originates from the low electronegativity (1.9) and the large atomic size ( $r_{\text{Ag}} = 1.442 \text{ \AA}$ ) of Ag atom.

Disregarding the accurate vertical positions of the oxygen atoms in the dark lines, which may be caused by the strong relaxation (V–V dimmer bond contracts by −40% [26]), the phase transition of the O–V(0 0 1) surface can be formulated as:

From V(0 0 1)–c(2 × 2)–2O<sup>1−</sup> ( $\Theta = 1/2 \text{ ML}$ , Fig. 1c):



to V(0 0 1)–( $\sqrt{2} \times 3\sqrt{2}$ )R45°–4O<sup>2−</sup> ( $\Theta = 2/3 \text{ ML}$ , Fig. 1e):



The first phase is exactly the same as the O–Rh(0 0 1) radial reconstruction. With increasing oxygen coverage, some O<sup>1−</sup> dislocates and all the O<sup>1−</sup> ions evolve into the O<sup>2−</sup> ions that gives rise to the ‘O–O’ zigzag chains and the short-ordered ( $\sqrt{2} \times 3\sqrt{2}$ )R45°–4O<sup>2−</sup> phase as shown in Fig. 1e, with V<sup>+/<sup>dipole</sup> specifying the bright protrusions.</sup>

There are two outstanding issues needing clarification. One is the inconsistency between the structures determined by LEED and by DFT/STM observations and the other is the oxygen coverage on the V(0 0 1) surface. AES detected higher oxygen coverage (0.67 and ~0.73 ML for the two phases, respectively) than

that required by the models (1/2 and 2/3 ML, respectively). The structural discrepancy may arise from the huge parameter space that guarantees not a unique solution [2]. Agreement between STM and DFT results may indicate the essentiality of searching for other possible numerical solutions in LEED optimization, such as the subsurface oxygen position. On the other hand, the V atoms in the center of the bright protrusions are expected to be missing as these atoms interact with no oxygen atoms but they experience strong repulsion from the neighboring V<sup>+/<sup>dipole</sup>. The expected missing V atoms may reduce the number of V atoms at the surface layers. In addition, the density of oxygen in the dark lines may be higher than the oxygen atoms inside the reconstructed domains. This may further increase the surface atomic ratio of O/V. These two factors would account for the difference in the O/V ratio between the AES measurement and the model specification. Further confirmation of the missing V atom formation is necessary.</sup>

The orders of the ionic bond formation at the Cu(0 0 1) and the (Rh, V, Ag)(0 0 1) surfaces are different owing to their atomic sizes and the values of electro-negativity. For instance, different patterns of O–Rh(0 0 1) and O–Cu(0 0 1) reconstruction arise from nothing more than the minor difference in their atomic sizes [radius, 1.342(Rh) – 1.277(Cu) = 0.065 Å] and electronegativity [2.2(Rh) – 1.9(Cu) = 0.3]. The smaller hollow [ $2R(\sqrt{2} - 1) = 1.058 \text{ \AA}$ ] and the lower electro-negativity of the Cu(0 0 1) surface allow the oxygen [ $d = 1.32 \text{ \AA}$ ] to bond to one Cu surface atom first, and then to another Cu underneath. The wider hollow [1.112 Å] and the higher electro-negativity of the Rh(0 0 1) surface permit oxygen to sink into the hollow and form the first bond to the Rh atom underneath. The inverse orders of ionic bond formation generate entirely different patterns of reconstruction and morphology, as well as the different surface atomic valences and phase structures on the fcc(0 0 1) surface of Cu, Rh, V, and Ag. Adsorption of oxygen to the Rh(0 0 1) surface creates the Rh<sub>5</sub>O radial and then the Rh<sub>4</sub>O tetrahedron that gives the ‘p4g’ clockwise reconstruction and the ‘rhombi-chain’ fashion. Oxygen reaction with the Cu(0 0 1) surface gives rise to the off-centered pyramid and then the missing-row structure in which the pairing ‘Cu<sup>dipole</sup>:O<sup>2−</sup>:Cu<sup>dipole</sup>’ strings form.

#### 4. Conclusion

We have applied the BBB correlation mechanism to compare the electronic process of the Ag(0 0 1) and V(0 0 1) surface oxidation compared with the O–Cu(0 0 1) and Rh(0 0 1) surface. Practice enables consistent insight into the bonding kinetics of these surfaces with the same fcc(0 0 1) geometry. The formulae of reaction with identification of atomic valencies and bond forming kinetics should provide complementary information to the knowledge obtained using the currently available state-of-the-art approaches. It is necessary to emphasize that although the patterns of observations using LEED and STM vary from situation to situation, formation of the primary oxide tetrahedron (sp-orbital hybridization), the bond forming kinetics ( $O^{1-} \rightarrow O^{2-}$ ) and the valence DOS (particularly the lone pair features) are the same for all the analyzed O–fcc(0 0 1) surfaces. However, the adsorbate site-specification, the order of the two ionic bond formation and the orientation of the oxide tetrahedron vary with the scale of the lattice and the value of electronegativity of the host, which determine the bond-order and the site-and-orientation specificity of the tetrahedron. As addressed previously, accurate determination of the static position of atoms seems not practical, as the reaction is a kinetic process in which charge polarization and charge transportation dominate and the involved atoms dislocate collectively and continually.

#### References

- [1] C.Q. Sun, *Prog. Mater. Sci.* 48 (2003) 521–685.
- [2] C.Q. Sun, *Surf. Rev. Lett.* 8 (2001) 367;  
C.Q. Sun, *Surf. Rev. Lett.* 8 (2001) 703.
- [3] C.Q. Sun, *Surf. Rev. Lett.* 7 (2000) 347.
- [4] C.Q. Sun, H. Xie, W. Zhang, H. Ye, P. Hing, *J. Phys. D* 33 (2000) 2196.
- [5] C.Q. Sun, Y.Q. Fu, B.B. Yan, S.P. Lau, X.W. Sun, B.K. Tay, *J. Appl. Phys.* 91 (2002) 2051.
- [6] C.Q. Sun, D. Jin, J. Zhou, S. Li, B.K. Tay, S.P. Lau, X.W. Sun, H.T. Huang, P. Hing, *Appl. Phys. Lett.* 79 (2001) 1082.
- [7] M. Kittel, M. Polcik, R. Terborg, J.T. Hoefl, P. Baumgartel, A.M. Bradshaw, R.L. Toomes, J.H. Kang, D.P. Woodruff, M. Pascal, C.L.A. Lamont, E. Rotenberg, *Surf. Sci.* 470 (2001) 311;  
T. Lederer, D. Arvanitis, G. Comelli, L. Troger, K. Baberschke, *Phys. Rev.* B48 (1993) 15390;
- A. Atrei, U. Bardi, G. Rovida, E. Zanazzi, G. Casalone, *Vacuum* 41 (1990) 333;
- M.C. Asensio, M.J. Ashwin, A.L.D. Kilcoyne, D.P. Woodruff, A.W. Robinson, T. Lindner, J.S. Somers, D.E. Ricken, A.M. Bradshaw, *Surf. Sci.* 236 (1990) 1;
- M. Wuttig, R. Franchy, H. Ibach, *J. Electr. Spec.* 44 (1987) 317.
- [8] W.M. Daniel, Y. Kim, H.C. Peebles, J.M. White, *Surf. Sci.* 111 (1981) 189;  
L.H. Dubois, *J. Chem. Phys.* 77 (1992) 5228;  
Y.G. Shen, A. Qayyum, D.J. O'Connor, B.V. King, *Phys. Rev.* B58 (1998) 10025;  
M. Zacchigna, C. Astaldi, K.C. Prince, M. Sastry, C. Comincioli, R. Rosei, C. Quaresima, C. Ottaviani, C. Crotti, A. Antonini, M. Matteucci, P. Perfetti, *Surf. Sci.* 347 (1996) 53;  
K. Ueda, A. Takano, K. Tanaka, *Jpn. J. Appl. Phys.* B34 (1995) 3662;  
A.G. Norris, F. Schedin, G. Thornton, V.R. Dhanak, T.S. Turner, R. McGrath, *Phys. Rev.* B62 (2000) 2113.
- [9] T. Fujita, Y. Okawa, Y. Matsumoto, K. Tanaka, *Phys. Rev.* B54 (1996) 2167.
- [10] H.C. Zeng, K.A.R. Mitchell, *Surf. Sci.* 239 (1990) L571.
- [11] F. Jensen, F. Besenbacher, E. Lagsgaard, I. Stensgaard, *Phys. Rev.* B42 (1990) 9206.
- [12] C.Q. Sun, *Vacuum* 48 (1997) 535.
- [13] J.R. Mercer, P. Finetti, F.M. Leibsle, R. McGrath, V.R. Dhanak, A. Baraldi, K.C. Prince, R. Rosei, *Surf. Sci.* 352–354 (1996) 173.
- [14] A. Baraldi, J. Cerdá, J.A. Martín-Gago, G. Comelli, S. Lizzit, G. Paolucci, R. Rosei, *Phys. Rev. Lett.* 82 (1999) 4874.
- [15] C.S.A. Fang, *Surf. Sci.* 235 (1990) L291.
- [16] M. Rocca, L. Savio, L. Vattuone, U. Burghaus, V. Palomba, N. Novelli, F.B. de Mongeot, U. Valbusa, R. Gunnella, G. Comelli, A. Baraldi, S. Lizzit, G. Paolucci, *Phys. Rev.* B61 (2000) 213.
- [17] G. Cipriani, D. Loffreda, A. Dal Corso, S. de Dironcoli, S. Baroni, *Surf. Sci.* 501 (2002) 182.
- [18] R. Koller, W. Bergermayer, G. Kresse, E.L.D. Hebenstreit, C. Konvicka, M. Schmid, R. Podloucky, P. Varga, *Surf. Sci.* 480 (2001) 11.
- [19] L. Savio, L. Vattuone, M. Rocca, V. de Renzi, S. Gardonio, C. Mariani, U. del Pennino, G. Cipriani, A.D. Corso, S. Baroni, *Surf. Sci.* 486 (2001) 65.
- [20] L.H. Tjin, M.B. Meinders, G.A. Sawatzky, *Surf. Sci.* 223 (1990) 341.
- [21] T.E. Felner, W.H. Weinberg, G.Y. Lastushkina, A.I. Boronin, P.A. Zhdan, G.K. Borskov, J. Hrbek, *Surf. Sci.* 118 (1982) 369.
- [22] F. Pforte, A. Gerlach, A. Goldmann, R. Matzdorf, J. Braun, A. Postnikov, *Phys. Rev.* B 63 (2001) 165405.
- [23] S. Warren, W.R. Flavell, A.G. Thomas, J. Hollingworth, P.L. Wincott, A.F. Prime, S. Downes, C. Chen, *J. Phys.: Condens. Matter* 11 (1999) 5021.
- [24] D. Alfe, S. de Gironcoli, S. Baroni, *Surf. Sci.* 410 (1998) 151.
- [25] C.Q. Sun, S. Li, *Surf. Rev. Lett.* 7 (2000) 213.
- [26] P.J. Feibelman, *Phys. Rev.* B53 (1996) 13740.